Measurement 137 (2019) 58–70

Contents lists available at ScienceDirect

Measurement

journal homepage: www.elsevier.com/locate/measurement

Estimating punching shear capacity of steel fibre reinforced concrete slabs using sequential piecewise multiple linear regression and artificial neural network

Nhat-Duc Hoang

Faculty of Civil Engineering, Institute of Research and Development, Duy Tan University, P809-03 Quang Trung, Da Nang, Viet Nam

ARTICLE INFO

Article history:
Received 9 October 2018
Received in revised form 22 December 2018
Accepted 14 January 2019
Available online 18 January 2019

Keywords:
Steel fibre reinforced concrete
Flat slab
Punching shear capacity
Sequential piecewise multiple linear regression
Artificial neural network

ABSTRACT

Estimating punching shear capacity is an important task in the design of steel fibre reinforced concrete (SFRC) flat slabs. The accuracy of commonly employed empirical design equations can potentially be improved with the use of machine learning. This study relies on a piecewise multiple linear regression (PMLR) and artificial neural network (ANN) approaches to construct a prediction model that can approximate the mapping function between the punching shear capacity of SFRC flat slabs and its influencing factors. Moreover, a sequential algorithm for automatically constructing the PMLR model structure is implemented. The algorithms of gradient descent and Levenberg-Marquardt backpropagation are employed to train the ANN based prediction models. A data set including 140 testing samples with six influencing factors of slab depth, effective depth of the slab, length or radius of the loading pad or column, compressive strength of concrete, the reinforcement ratio, and the fibre volume have been collected from the literature. This data set is then used to train and verify the sequential PMLR (SPMLR) and ANN models. Experimental results show that SPMLR can deliver prediction outcome which is better than those of ANN as well as empirical design equations. Therefore, SPMLR can be a promising alternative to assist structural engineers in the design phase of structures containing SFRC flat slabs.

1. Introduction

Reinforced concrete flat slabs are the structural elements which are widely utilized in various types of civil engineering projects including parking stations, office blocks, and residential buildings. It is because the structure of cast-in-place two-way concrete slabs can provide architects and engineers with an economical structural system [1,2]. As pointed out in [3], the characteristics of reinforced concrete flat slabs, e.g. the flat soffit, significantly ease the tasks of formwork and rebar installations. These structures also allow the reduction of the overall storey heights.

The advantages and convenience of using reinforced concrete flat slabs have drawn attentions of many scholars who have studied the behavior of these structures both in analytical and experimental manners [4–6]. Previous studies clearly point out that the ultimate strength of a reinforced concrete flat slab is typically determined by the punching shear capacity at its slab-column connections [2]. Moreover, post-punching residual strength of a slab is considerably smaller than the punching load. Hence, after the slab is punched at one column, its adjacent columns are quickly overloaded and reach the state of failure on punching. This phenomenon is capable of triggering the progressive collapse of buildings that employs flat slab structures [2].

By reviewing the literature, it can be seen that many building collapses caused by failures on punching are reported. Human casualties and considerable economic loss have also been observed. Schousboe [7] reports the case of failure of a 24-story building under construction at Bailey's Crossroads (Virginia) in 1973; post-failure investigation points out that the building collapses is triggered by a shear failure in the slab structure on the 23rd floor. In another study, [8] reports the collapse of a 16-story apartment building constructed in Boston (Massachusetts) which is also due to low punching shear strength of the flat slab structure.

These structural collapses motivate recent studies on the failure mechanism of the structure, enhancing the slab punching shear capacity, as well as meliorating the design process of flat slabs governed by conventional empirical formulas. Since steel fibers have become increasingly popular in structural engineering [9], it has been used as a reinforcement in concrete flat slab to enhance the punching shear capacity [10–12]. Based on previous experimental works [3], the enhancement of the punching shear capacity of steel fiber reinforced concrete (SFRC) flat slabs have been confirmed.

E-mail address: hoangnhatduc@dtu.edu.vn

https://doi.org/10.1016/j.measurement.2019.01.035
0263-2241/

This fact sparks the wide employment of SFRC flat slabs in civil engineering structures.

Nevertheless, the current design codes for slab–column connections (e.g. ACI 318-11 [13]) have been originally established for normal concrete structures and the applications of existing codes obviously need adaptations to suit the design process of SFRC slabs. Narayanan and Darwish [14] proposed an equation for determination of the punching shear capacity of SFRC slabs by taking into account the strength of the compressive zone over the inclined cracks, the pull-out shear forces on the steel fibres along these cracks, and the shear forces supported by membrane actions. Another design equation has been put forward by Harajli, Maalouf and Khatib [15] which is based on linear regression; this statistical approach is employed to analyze the contribution of concrete and fibres on the overall punching shear strength.

Choi et al. [16] carried out theoretical study to investigate the performance of a design equation based on the assumption regarding the behavior of tensile reinforcement prior to punching shear failures. Maya, Fernández Ruiz, Muttoni and Foster [3] collected available experimental data in the literature to verify and compare three predictive equations used for computing the punching shear capacity. An experimental study has been performed in [17] to investigate the behaviour of SFRC flat slabs up to failure under a concentrated loading. Gouveia, Lapi, Orlando, Faria and Ramos [18] recently performed an experimental study to evaluate the punching shear capacity of SFRC slab–column connections. Experimental research works on the behaviour and load capacity of steel fibre-reinforced concrete (SFRC) flat slabs under monotonically increased concentrated vertical loads and reversed horizontal cyclic loading have been carried out in [19] and [20].

Kueres, Ricker, Classen and Hegger [21] studied the punching shear behavior of reinforced concrete flat slabs and column bases using fracture kinematics of slabs failing in punching. A two-parameter kinematic theory for punching shear in reinforced concrete slabs without shear reinforcement has been established in [22]. Einpaul, Ruiz and Muttoni [23] put forward a novel experimental method for tracking the formation and development of cracks inside punching test specimens. An analysis of measurements on the kinematics and crack development associated with punching failures has been carried out in [24]; the analysis results were then employed to formulate a mechanical model for better understanding punching shear failures.

As can be seen from the current literature, the prediction of shear punching capacity of SFRC is mainly focused on the use of adapted design equations and simple statistical method. Although theoretical prediction models are crucial to investigate the relationship between shear punching capacity of SFRC and its influencing factors, punching shear behavior is a complex phenomenon and other estimation approaches should be worth investigating. Since the mechanism that governs shear punching capacity of flat also involves many influencing variables, the investigation of other advanced data-driven methods is necessary to enhance the prediction performance and enrich the body of knowledge.

Because machine learning has been increasingly popular in the community of structural engineering [25–30], this study proposes the utilization of this advanced data analysis method in shear punching capacity estimation. Piecewise linear multiple regression (PLMR) and artificial neural network (ANN) are selected to be employed to construct shear punching capacity estimation models for SFRC flat slabs. In addition, a sequential and automatic method is employed to train the PLMR model. The ANN model is constructed via the algorithms of gradient descent backpropagation and Levenberg-Marquardt backpropagation.

In this study, there is a focus on the former machine learning model. It is because structure of the PLMR model can be explicitly described, visualized, and interpreted. These advantages of PLMR make this machine learning approach a suitable tool for structural engineers in modeling shear punching capacity. The latter approach of ANN is a powerful nonlinear modeling tool [31,32]; however, it is a black-box model meaning that its structure can hardly be described and interpreted by human. The performances of PLMR and ANN are compared to those of multiple linear regression and empirical equations to identify the most capable prediction approach.

A dataset including 140 experimental data samples, collected from the literature, has been used to train and verify the aforementioned machine learning models. In this data set, six explanatory variables including slab depth, effective depth of the slab, length or radius of the loading pad or column, compressive strength of concrete, the reinforcement ratio, and the fibre volume are employed to make inference on the measured punching shear strength. The rest of the paper is organized in the following sequence. The second section reviews the research methodology, followed by a section that clearly describes the iterative procedure used to determine the structure of the PLMR model. Experimental results are reported in the fourth section, followed by the last section which summarizes the current study with several concluding remarks.

2. Research methodology

2.1. Piecewise multiple linear regression (PMLR)

Multiple linear regression (MLR) is a widely employed data modeling approaches which applications span various domains [33]. Given the collected data, this method can be used to express a relationship between a set of explanatory variable X and a response variable Y in form of a meaningful predictive equation. However, MLR cannot deal effectively with complex and nonlinear data due to its respected assumption on linear relationships among variables [34]. To preserve the advantage of the conventional MLR and to equip it with nonlinear modeling capability, researchers and practitioners have resorted to PMLR [35,36].

A PMLR is a data modeling method that employs each linear model to fit a subset of the input data X (see Fig. 1). The transition location from a certain explanatory variable domain to another explanatory domain is termed as a breakpoint (also called a knot). A break point or a knot is defined as the value of the explanatory variable where the linear functions intersect [34]. The break point locations allow the overall learning space to be disintegrated into subspaces within which multiple linear models can be used to represent an overall nonlinear data mapping. Generally, the appropriate value of a knot is unknown and must be estimated from the collected data set.

The mathematical formula of a PMLR with one knot is given as follows [36]:

$$Y(X_i) = \begin{cases} \sum_{d=1}^{D+1} \beta_d X_{i,d} & \text{if } X_{i,d} \leqslant b \\ \sum_{d=1}^{D+1} \beta_d X_{i,d} & \text{if } X_{i,d} > b \end{cases} \quad (1)$$

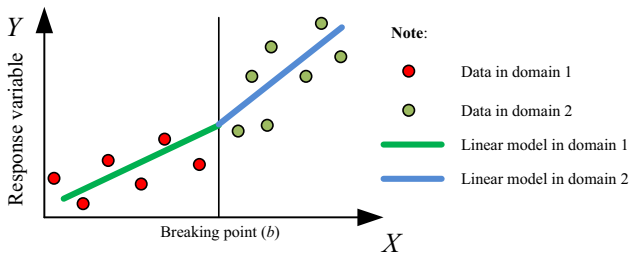

Fig. 1. Piecewise linear regression model.

where X_i is the vector of the ith explanatory variable consisting of D elements. b is the breaking point value. Y is the response variable.

Moreover, for each linear model, the least square method can be used to estimate the model parameter β. The least square estimate of β is determined so that the residual sum of squares function is minimized [33]:

$$\text{Minimize } RSS(\beta) = \sum_{i=1}^{N} (Y_i - X_i\beta^T)^2 \tag{2}$$

The least squares estimation of the linear model parameter β is β_* which is given as [33]:

$$\beta_* = (X^T X)^{-1} X^T Y \tag{3}$$

where X is the matrix of explanatory variables; X has the size Nx(D + 1), where N is the number of data instances and D is the number of explanatory variables. Y with the size of Nx1 is the vector containing values of the response variable.

The aforementioned model can be extended to the case in which there is more than one breaking point. The crucial task is how to automatically locate the breaking points for each explanatory variable. Previous works have dedicated in solving this task by formulating it as a mathematical programming problems. However, some of the methods are only applicable for data set involving one explanatory problems [37–39]; other methods [40–42] are mathematically intensive and this fact imposes a significant challenge for practicing structural engineers to implement. Therefore, in the third section, a simpler algorithm is presented to automatically identify the breaking points and construct the PMLR model in a sequential manner.

2.2. Artificial neural network (ANN)

In structural engineering, ANN is widely considered as a capable nonlinear tool for modeling complex processes which require the analyses of multiple explanatory variables [43]. Successful applications of ANN have been extensively reported by various scholars and practitioners in structural engineering field [44–46]. An ANN attempts to mimic the information acquisition, information processing, and knowledge generalization occurred in human brain. In the particular application of punching capacity estimation, an ANN learns from the results of experimental tests of SFRC flat slabs to infer a mapping function that determines their punching capacity.

The structure of an ANN model used for punching capacity estimation is illustrated in Fig. 2. An ANN model is an interconnected network of simple neurons. Even though the learning and generalization capability of an individual neuron is limited, the combined structure of an ANN model possesses the capability of universal learning [47]. This fact indicates that an ANN model equipped with a sufficient number of neurons in its hidden layer can approximate any unknown function or process with arbitrary accuracy.

The target herein is to approximate a hidden function $f : X \in R^{NX} \rightarrow Y \in R^1$ (where NX is the number of input attributes) that determines the mapping between a set of explanatory variables and the response variable of the punching shear capacity. To do so, an ANN model structure consisting of an input, a hidden, and an output layer is used. Since slab depth, effective depth of the slab, length or radius of the loading pad or column, compressive strength of concrete, the reinforcement ratio, and the fibre volume are used to predict values of the response variable, NX = 6 which is the number of the input neurons. Moreover, there are no strict rules to determine NR which is the number of neurons in the hidden layer. In this study, the suitable value of NR is searched in the range of 3–10 neurons; the value of NR which results in the highest predictive performance of the ANN model is selected.

Notably, the training process of an ANN involves the adaptation of its parameters consisting of the weight matrix of the hidden layer (W_1), the weight matrix of the output layer (W_2), the bias vector of the hidden layer (b_1), and the bias vector of the output layer (b_2). The values of these matrices and vectors are selected to provide the best fit to the collected data set. Moreover, f_A in Fig. 1 represents an activation function for each neuron in the hidden layer, the sigmoid function is often employed [48] as activation function for ANN; this function is shown as follows:

$$f_A(n) = \frac{1}{1 + e^{-n}} \tag{4}$$

To train a network structure, the algorithm of error backpropagation is widely employed. In addition, the Mean Square Error (MSE) loss function is often used in the training phase of an ANN employed for function approximation tasks [48]:

$$MSE = \min_{W_1, W_2, b_1, b_2} \frac{1}{M} \sum_{i=1}^{M} e_i^2 \tag{5}$$

where M denotes the number of training samples; e_i is the deviation between the observed and the predicted values of the punching

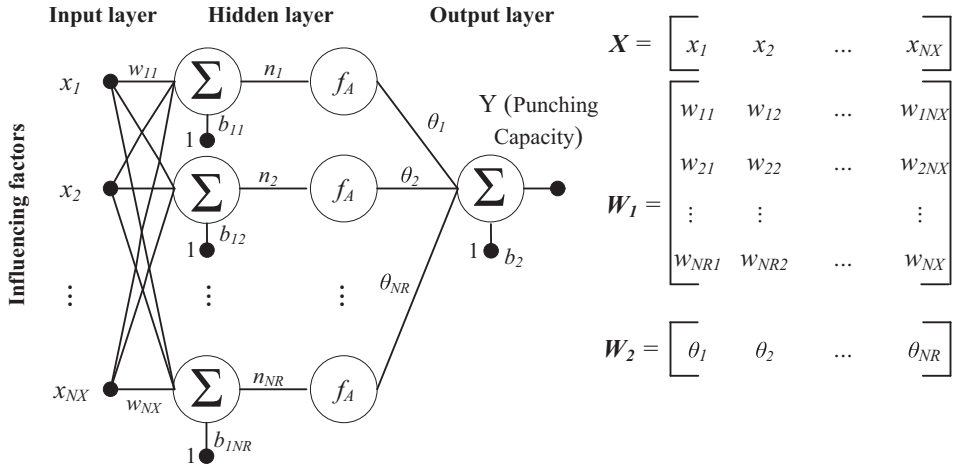

Fig. 2. A typical structure of an ANN.

shear capacity: $e_i = Y_{i,P} - Y_{i,A}$; $Y_{i,P}$ and $Y_{i,A}$ represent the predicted and actual values of the punching shear capacity, respectively.

To minimize the loss function and construct the ANN model used for estimating the punching shear capacity, the algorithms of gradient descent backpropagation [49,50] and Levenberg-Marquardt backpropagation [51,52] are employed. The former algorithm has been programmed by the author in MATLAB programming environment, the latter algorithm is implemented via the MATLAB Statistics and Machine Learning Toolbox [52].

2.3. The experimental dataset

To train and verify the models of PMLR and ANN, a data set including 140 testing samples and six punching capacity governing factors of the slab depth (X_1), effective depth of the slab (X_2), length or radius of the loading pad or column (X_3), compressive strength of concrete (X_4), the reinforcement ratio (X_5), and the fibre volume (X_6). The data samples are collected from the previous experimental works in the literature and have been summarized by Maya, Fernández Ruiz, Muttoni and Foster [3]. The statistical characteristics of the variables in the data set are summarized in Table 1. The histograms of both explanatory and response variables are illustrated in Fig. 3.

3. Sequential piecewise multiple linear regression model for estimating punching shear capacity of SFRC flat slabs

This section of the study describes the proposed model of Sequential Piecewise Multiple Linear Regression (SPMLR) for predicting punching shear capacity of SFRC flat slabs. The overall model structure is presented in Fig. 4. It is noted that the model has been programmed by the author in MATLAB programming environment. Moreover, SPMLR takes the aforementioned six factors of the slab depth (X_1), effective depth of the slab (X_2), length or radius of the loading pad or column (X_3), compressive strength of concrete (X_4), the reinforcement ratio (X_5), and the fibre volume (X_6) as input information to derive the output of punching shear strength.

In the step of Break Point set initialization, each input attribute X_d is divided into K_P equally spaced intervals within the range of $\max(X_d)$ and $\min(X_d)$: $\min(X_d) < k_{d,1} < k_{d,2} < \ldots < \max(X_d)$. Thus, each input attribute has $K_P + 1$ candidates of break points or knot. The values of Kp is selected from the set ranging from 50 to 500 with an interval of 50, the value of K_p results in the most desired model accuracy is chosen.

The model formulation of the SPMLR model is based on the concept of a hinge function [53] (see Fig. 5). A hinge function returns a value of zero for a certain part of its range. Hence, this function can be used to partition the data into separated region; each of the separated regions has distinctive properties and can be fitted by an individual linear model. Using such concept, a SPMLR model with one explanatory variable X and one break point or knot b is presented in the following form:

$$Y = \beta_o + \beta_{11}\max(0, sign(X-b)) + \beta_{12}\max(0, sign(b-X)) + \beta_{21}\max(0, X-b) + \beta_{22}\max(0, b-X) \quad (6)$$

Thus, the functional formula of $Y(X)$ according to different value of X can be expressed as follows:

- If X > b then $Y = \beta_{11} + \beta_{21}\max(0, X-b)$
- If X < b then $Y = \beta_{12} + \beta_{22}\max(0, b-X)$
- If $X = b$ then $Y = \beta_0$.

Basically, for each knot b of the variable X, two linear models are used to fit the data set at the two sides of the breaking point b. The terms β_0, β_{11}, and β_{12} are the bias parameters; the terms β_{21} and β_{22} are the slope parameters of the two linear models. The simple model with one explanatory variable and one breaking point can be extended to a model with many explanatory variables and multiple breaking points as follows:

$$Y = \sum_{d=1}^{D}\sum_{v=1}^{V_d} LF_{d,v}(X_d) \quad (7)$$

where d denotes the index of explanatory variables; D is number of explanatory variables; v is the index of the hinge function of the dth explanatory variable; V_d is the number of hinge functions of the dth explanatory variable.

The model is built sequentially by seeking for an appropriate breaking point of each explanatory variable in each iteration. For each influencing factors of the punching shear capacity, the breaking point value is searched from a set of values ranging from the minimum and maximum values of the factor. As mentioned earlier, that the set of values is constructed as a row vector of K_{P+1} evenly spaced points between the minimum and maximum values of the factor. The model construction phase of SPMLR is illustrated in Fig. 6.

To accept or reject a knot candidate, this study proposes to employ the following three break point acceptance criteria; each acceptance criterion (AC) is given as follows:

$$\text{AC 1}: f_{AC} = \text{RMSE}_{TR} + \text{RMSE}_{VA} \quad (8)$$

$$\text{AC 2}: f_{AC} = R - \text{RMSE}_{TR} \quad (9)$$

$$\text{AC 3}: f_{AC} = R - \text{RMSE}_{TR} + R - \text{RMSE}_{VA} \quad (10)$$

The AC relies the computed function value of f_{AC} to quantify the contribution of a knot candidate to the reduction of the overall model error. If the inclusion of a breaking point leads to reduction in model error, this breaking point candidate is accepted to enter the model structure. Herein, the Root Mean Square Error (RMSE) is used to express the model prediction error; the formula used to compute RMSE is shown as follows:

$$RMSE = \sqrt{\sum_{t=1}^{N}\frac{(Y_{A,i} - Y_{P,i})^2}{N}} \quad (11)$$

Table 1
Statistical characteristics of the variables.

Variables	Notation	Description	Min	Mean	Median	Std	Skewness	Max
X_1	h (mm)	The slab depth	55.00	110.82	125.00	33.22	−0.37	180.00
X_2	d (mm)	The effective depth of the slab	39.00	87.05	100.00	28.66	−0.30	150.00
X_3	b_c (mm)	The length or radius of the loading pad or column	60.00	131.96	150.00	46.33	0.31	225.00
X_4	f_c (Mpa)	The compressive strength of concrete	14.20	41.65	36.85	21.30	1.93	108.00
X_5	ρ (%)	The reinforcement ratio	0.37	0.99	0.85	0.51	0.82	2.53
X_6	ρ_f (%)	The fibre volume	0.00	0.71	0.80	0.48	0.24	2.00
Y	V (kN)	The measured punching shear strength	58.30	228.20	219.60	110.56	0.60	530.00

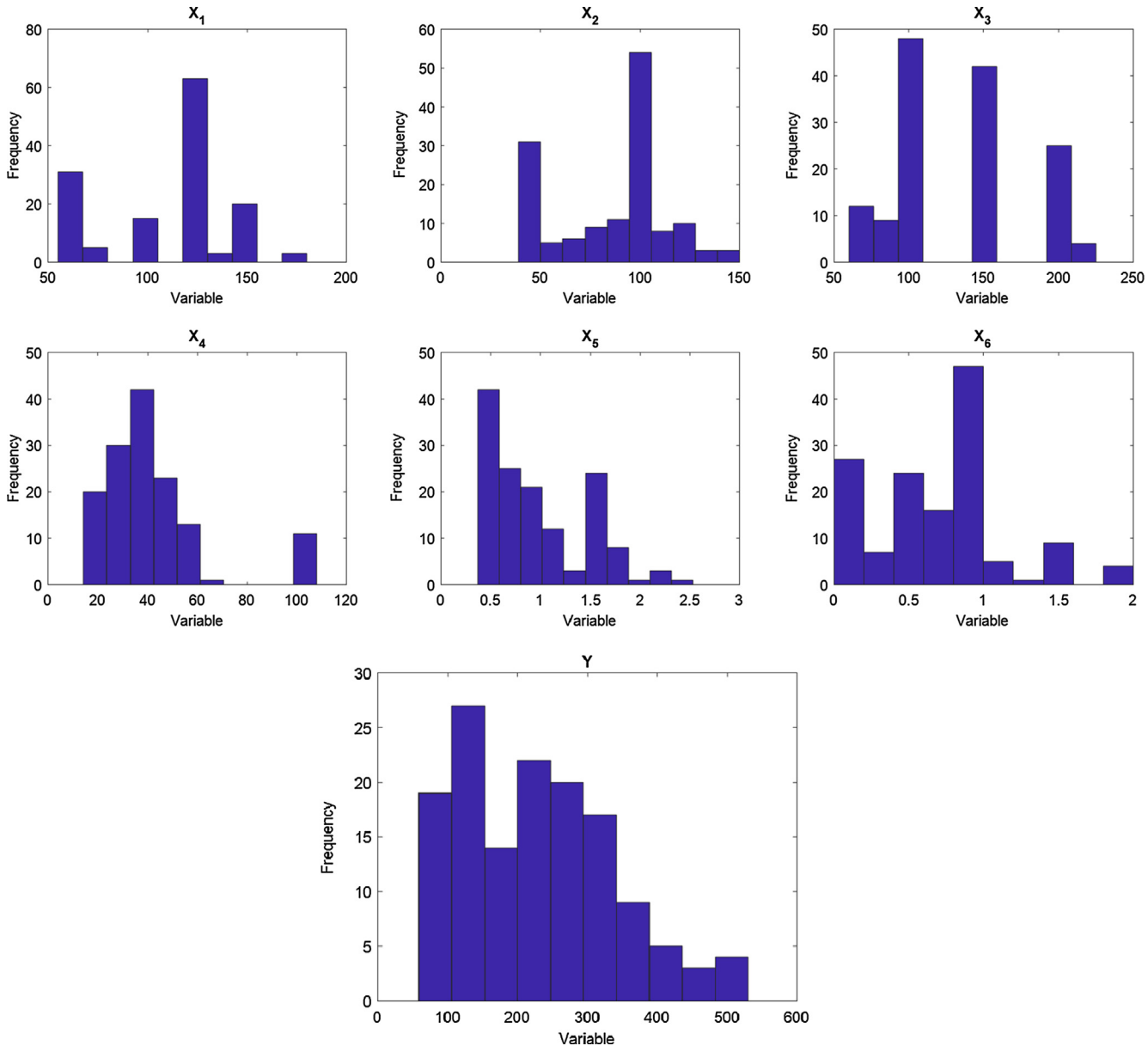

Fig. 3. Histograms of the explanatory variables and response variable.

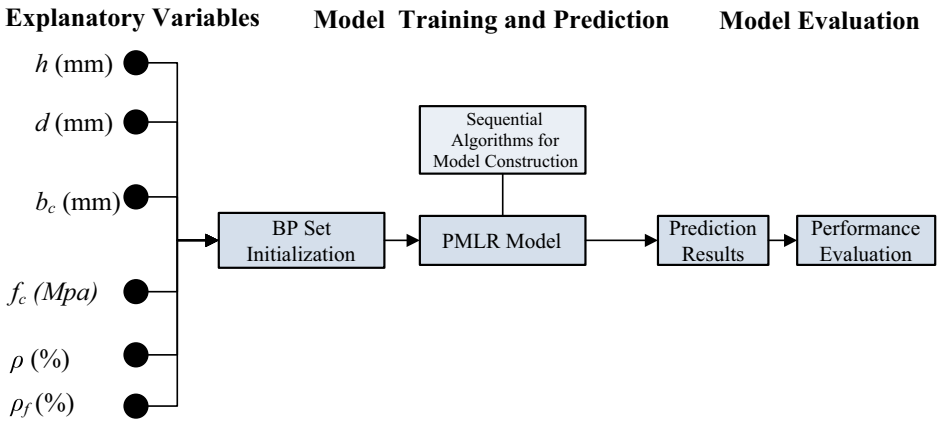

Fig. 4. The proposed model structure.

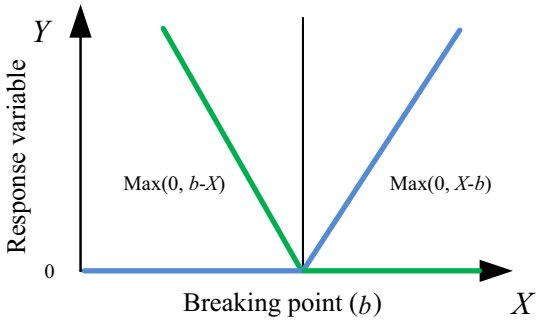

Fig. 5. The proposed model structure.

Define the breaking point acceptance criterion (AC)
Define the maximum number of iterations *I_Max*
For *iter* = 1 to *I_Max*
  Initialize Model_Structure = []
  For *d* = 1 to *D* // *D* is the number of explanatory variables
    For *v* = 1 to *Vd* // *Vd* is the number of hinge functions
      Identify a breaking point for *Xd* based on AC
      Update Model_Structure
      Compute Model_Parameter β using least squares estimation
    End For
  End For
End For
Return Model_Structure and Model_Parameter

Fig. 6. The model construction phase.

where $Y_{A,I}$ and $Y_{P,I}$ denote the actual and the predicted output of the i^{th} data sample, respectively. N is the number of data samples in the current data set of interest.

In Eq. (14), the AC function takes into account RMSE values of both training and validating data. Herein, the original data set has been divided into three separated subsets: training set (80%), validating set (10%), and testing set (10%). The first two subsets are employed in the model construction phase; the last subset is reserved to confirm the model predictive capability. It is noted that the incorporation of the validation data set into f_{AC} is to guard against overfitting. Overfitting easily occurs during the data fitting process if the model becomes too complex and fits the training data set so well but performs poorly on novel data. Thus, the inclusion of the validating prediction error is one way to alleviate the overfitting problem.

Besides the approach described in Eq. (14), two other forms of f_{AC} is introduced in Eq. (15) and Eq. (16). With the observation that the model complexity can be expressed by the number of accepted breaking points, the Regularized Root Mean Square Error (R-RMSE) can be used to combine both the model accuracy and complexity as follows:

$$R-RMSE=\sqrt{\sum_{t=1}^{N}\frac{(Y_{A,i}-Y_{P,i})^2}{N}}+\frac{BPN}{N} \tag{12}$$

where *BPN* denotes the number of breaking points or knots. N is the number of data samples in the current data set of interest.

Eq. (15) only computes the value of R-RMSE for the training data set. Meanwhile, Eq. (16) considers the values of R-RMSE for both training data set and validating data set. Moreover, to balance the two objectives of minimizing the prediction error and maximizing the model generalization, it is experimentally found that the value of BPN must be multiplied by a coefficient μ_{BPN} to reduce its original value. In this study, via a trial-and-error computing process, the suitable value of μ_{BPN} can be roughly set to be $1/N$ where N is the number of data samples in the training set. After the model construction phase is finished, the model structure of a SPMLR, including knots of each explanatory variable and the vector of model parameters β, can be identified. Accordingly, the model is ready for predicting data instances in the testing set.

4. Experimental results

In this section of the study, the performance of the proposed SPMLR model is compared to that of the ANN models. Moreover, the prediction result of the multiple linear regression model (MLR) as a standard tool in statistical modeling is also included in the result comparison. To reliably assess the model prediction outcome, a repetitive random subsampling including 20 training and testing times has been performed. In each run, 90% of the data is used for training the punching shear strength estimation model and 10% of the data is used as testing cases.

Moreover, to appraise the performance of the model, besides RMSE, the mean absolute percentage error (MAPE), the mean absolute error (MAE), and the coefficient of determination (R^2) are utilized. The formulas used to compute these three performance measurement indices are shown as follows:

$$MAPE=\frac{100\%}{N_d}\sum_{t=1}^{N_d}\frac{|Y_{A,i}-Y_{P,i}|}{Y_{A,i}} \tag{13}$$

$$MAE=\frac{1}{N_d}\sum_{t=1}^{N_d}|Y_{A,i}-Y_{P,i}| \tag{14}$$

$$R^2=\frac{SS_{yy}-SSE}{SS_{yy}} \tag{15}$$

where $Y_{A,i}$ and $Y_{P,i}$ denote the actual and the predicted values of the punching shear capacity of the i^{th} data instance. N_d represents the number of data instances in the set of interest.

To calculate R^2, SS_{yy} and SEE are obtained via the following equations:

$$SS_{yy}=\sum_{i=1}^{N}(Y_{A,i}-Y_{A,m})^2 \tag{16}$$

$$SSE=\sum_{i=1}^{N}(Y_{A,i}-Y_{P,i})^2 \tag{17}$$

where $Y_{A,m}$ denotes the mean value of actual punching shear capacity.

The prediction results of the SPMLR models according to different AC obtained from the repetitive random subsampling process are presented in Table 2. In this table, the mean and the standard deviation (Std) of the outcomes are reported. It can be seen that the SPMLR model employing AC 3 has achieved the best prediction accuracy with RSME = 27.47, MAPE = 11.21%, MAE = 21.52, and R^2 = 0.95. Based on the experimental result, it is able to conclude that the inclusion of model performance on the validating data and the number of accepted knots for quantifying the model complexity can help to achieve good prediction accuracy on punching shear strength estimation.

Moreover, the appropriate maximum number of iterations *I_Max* of the SPMLR models using AC 1, 2, and 3 (see Fig. 6) are found to be 1, 2, and 2, respectively. The SPMLR models employ *I_Max* larger than those reported values get overfitted and obtain inferior testing results. The prediction result of the SPMLR model using AC 2 and *Iter_Max* = 2 are demonstrated in Fig. 7.

The results of the SPMLR model, ANN models, and MLR model obtained from the repeated random subsampling process with 20 runs are reported in Table 3. Since the SPMLR model with AC 2 and the maximum number of iteration = 2 has attained the best

Table 2
Performance of the SPMLR models with different break point AC.

Phase	Performance	SPMLR (AC 1)		SPMLR (AC 2)		SPMLR (AC 3)	
		Mean	Std	Mean	Std	Mean	Std
Training	RMSE	23.25	2.13	17.80	1.52	16.18	0.83
	MAPE (%)	9.30	0.83	7.27	0.51	6.69	0.26
	MAE	17.96	1.76	13.70	1.07	12.56	0.63
	R^2	0.96	0.01	0.97	0.00	0.98	0.00
Testing	RMSE	33.65	12.94	30.77	16.16	27.47	7.80
	MAPE (%)	12.00	4.07	11.28	4.69	11.21	3.35
	MAE	24.72	7.36	22.33	8.52	21.52	4.32
	R^2	0.91	0.06	0.92	0.08	0.95	0.04

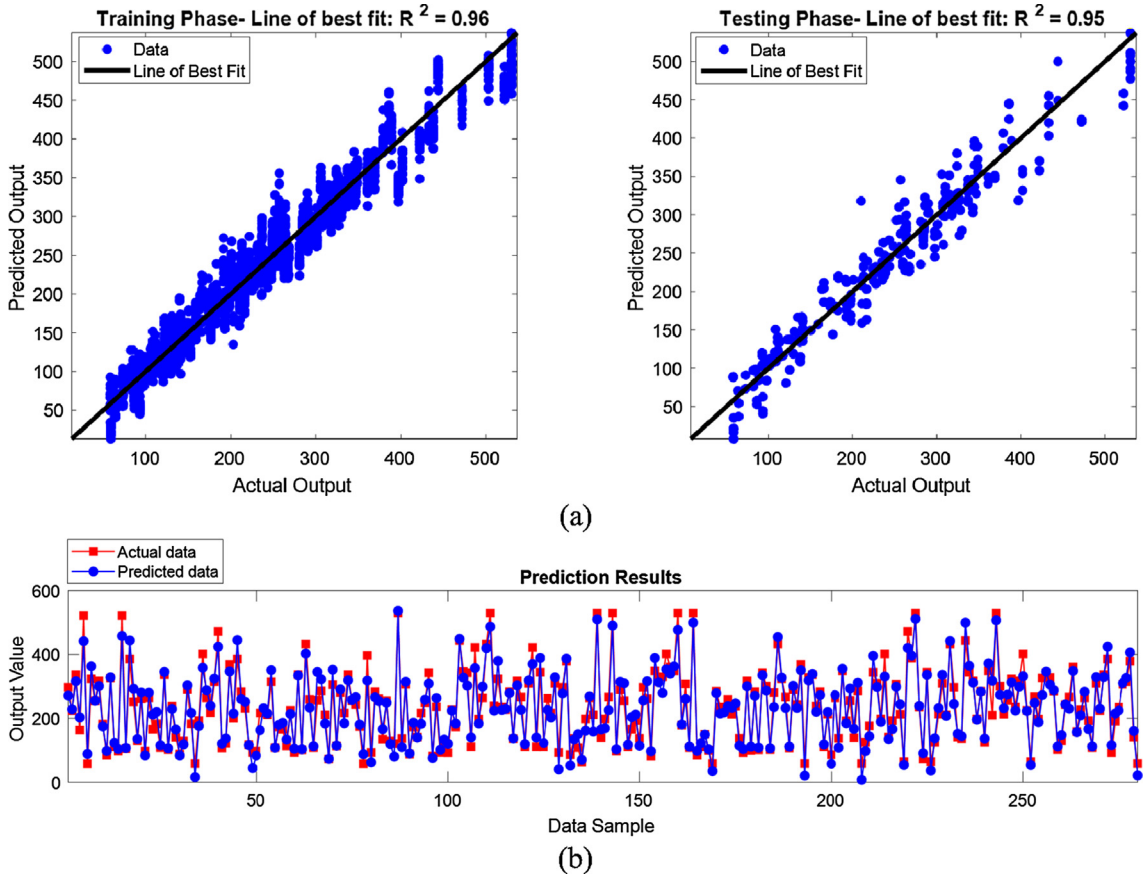

Fig. 7. Prediction performance of the SPMLR model using AC 2 and *Iter_Max* = 2: (a) Deviation around the line of best fit and (b) The actual vs. the predicted outcomes.

Table 3
Performance comparison of the prediction models.

Phase	Performance	Prediction Models							
		SPMLR		GD-BPANR		LM-ANR		MLR	
		Mean	Std	Mean	Std	Mean	Std	Mean	Std
Training	RMSE	21.95	2.92	20.74	2.37	29.63	8.70	166.46	9.38
	MAPE (%)	8.74	1.07	7.73	0.75	10.85	3.48	96.23	6.57
	MAE	16.97	2.18	15.34	1.73	21.69	6.74	146.41	8.80
	R^2	0.96	0.01	0.97	0.01	0.93	0.04	0.63	0.01
Testing	RMSE	27.47	5.22	33.16	8.91	35.78	15.06	167.60	18.35
	MAPE (%)	11.21	2.79	12.04	2.73	13.73	8.03	99.20	24.72
	MAE	21.52	3.79	24.90	5.83	26.38	9.84	146.38	18.55
	R^2	0.95	0.03	0.91	0.06	0.90	0.09	0.64	0.12

prediction results, this model is used for the purpose of result comparison. As described earlier, the two ANN models are trained by the algorithms of gradient descent backpropagation and Levenberg-Marquardt backpropagation; they are respectively denoted as GD-BPANR and LM-ANR. The performances of the two ANN models in their training and testing phases are also illustrated in Fig. 8.

Observed from Table 3, the performance of SPMLR (RSME = 27.47, MAPE = 11.21%, MAE = 21.52, and R^2 = 0.95) is better than those of GD-BPANR (RSME = 33.16, MAPE = 12.04%, MAE = 24.90, and R^2 = 0.91), LM-ANR (RSME = 35.78, MAPE = 13.73%, MAE = 26.38, and R^2 = 0.90), and MLR (RSME = 167.60, MAPE = 99.20%, MAE = 146.38, and R^2 = 0.64). The poor result of MLR strongly indicates that the actual mapping between the input attributes and the values of punching shear capacity is highly nonlinear and simple linear relationship cannot be sufficient to capture such mapping.

Based on the experimental results, the SPMLR model employing AC 2 has outperformed other benchmark prediction models. This model is retrained with the whole collected data set including 140 samples; the results obtained from this SPMLR model is then compared to those of prediction equations described in [3]. It is proper to note that the SPMLR model is also trained with the maximum number of iteration = 2. The three employed prediction equations described in [3] are denoted as Pred. Eq. A, B, and C. As can be seen from Table 4 which reports the result comparison, SPMLR has outperformed all the prediction equations. Compared to the best prediction equation (Pred. Eq. A), SPMLR has gained a 21% improvement in RMSE, 9% improvement in MAPE, and 23% improvement in MAE. In terms of R^2, the result of SPMLR (0.96) is also higher than the best prediction equation (0.94).

Based on the experimental outcomes, it is able to conclude that SPMLR is a highly suited approach for modeling the punching shear strength of SFRC flat slabs. Moreover, based on the training result, the breaking point values of each explanatory variable found by SPMLR are illustrated in Fig. 9. It can be seen that the variable X_3, X_5, and X_6 has only one breaking point; the other variables require two breaking points. In addition, the identified model

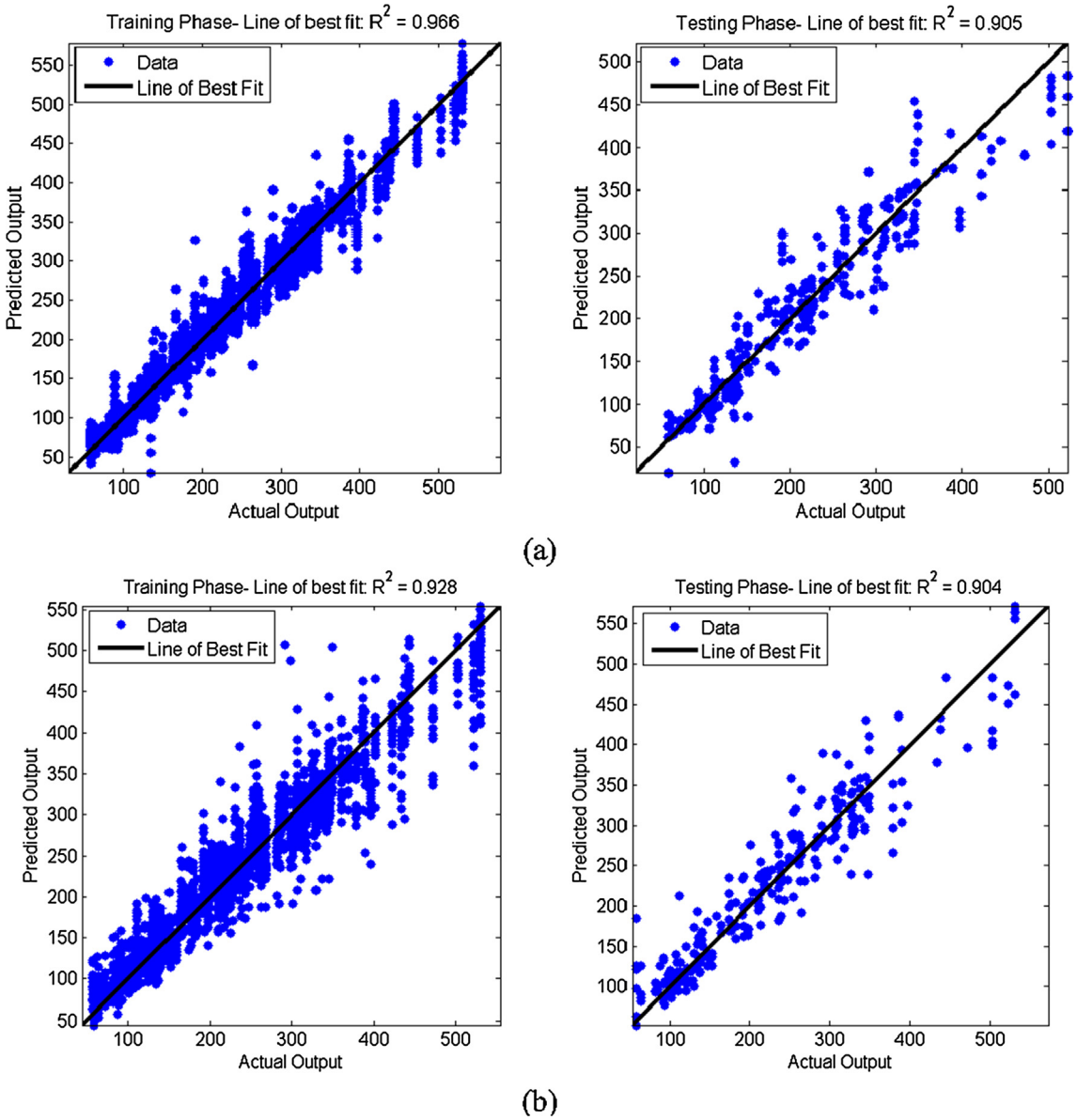

Fig. 8. Prediction performances of neural network models: (a) GD-BPANR and (b) LM-BPANR.

Table 4
Comparison between machine learning models and prediction equations.

Performance	Pred. Eq. A	Pred. Eq. B	Pred. Eq. C	SPMLR
RMSE	26.18	34.91	56.66	20.78
MAPE (%)	8.81	11.85	20.46	7.98
MAE	20.46	28.01	47.23	15.76
R^2	0.94	0.90	0.74	0.96

Note: The descriptions of the employed prediction equations are provided in Appendix 1.
Pred. Eq. A: using Eq. (A1) for concrete contribution and Eq. (A4) for fibres contribution
Pred. Eq. B: using Eq. (A1) for concrete contribution and Eq. (A5) for fibres contribution.
Pred. Eq. C: using Eq. (A6) for concrete contribution and Eq. (A5) for fibres contribution.

structure of SPMLR including the breaking points and the model parameter β are reported in Table 5.

To demonstrate that SPMLR can be a useful tool for visualizing the relationship among variables in the task of modeling the punching shear strength of SFRC flat slabs, the relationship among reinforcement ratio, fibre volume, and punching shear strength is provided in Fig. 10 as an example. The four samples with fiber volume (X_6) = 0, 0.5, 1.0, and 1.5 are randomly extracted from the collected data set and presented as follows:

Case 1 (Fig. 10a): $X_1 = 152$, $X_2 = 127$, $X_3 = 152$, $X_4 = 47.7$, $X_5 = 0.98$, $X_6 = 0$, and $Y = 433$.

Case 2 (Fig. 10b): $X_1 = 125$, $X_2 = 100$, $X_3 = 150$, $X_4 = 34$, $X_5 = 0.56$, $X_6 = 0.5$, and $Y = 225$.

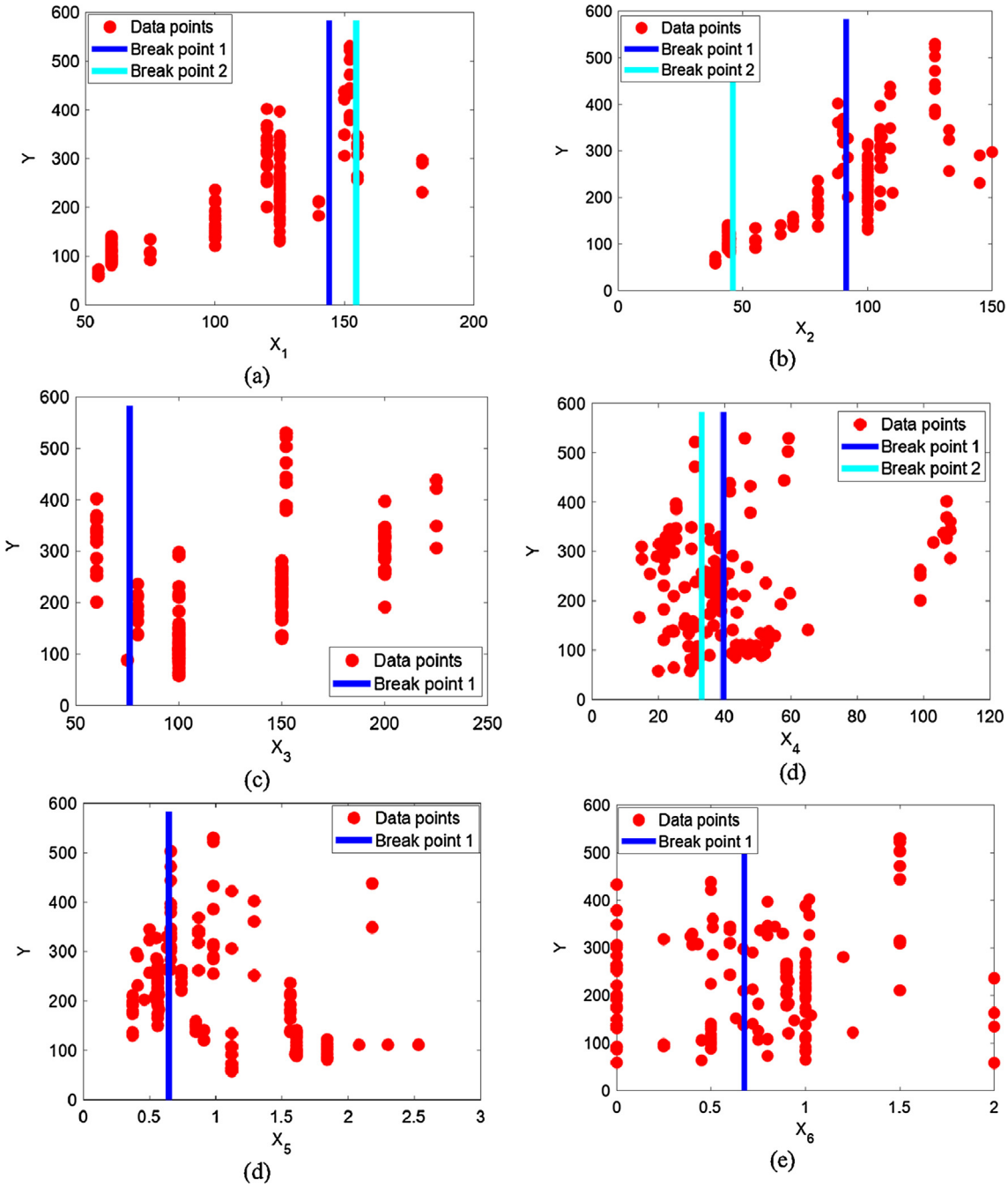

Fig. 9. Break points of SPMLR model: (a) X_1, (b) X_2, (c) X_3, (d) X_4, (e) X_5, and (f) X_6.

Table 5
The SPMLR model structure.

Explanatory Variables	Break point set (Z-score transformed)	Break point set (Converted to original range)	Parameter of linear regression models (β)				
X1	1.00	144.05	0.00	0.00	2.86	0.00	14.60
	1.31	154.50	0.00	0.00	1.97	0.28	−14.70
X2	0.15	91.34	0.00	0.00	0.08	0.84	−0.86
	−1.43	46.05	0.00	0.19	0.00	−0.13	1.69
X3	−1.21	76.00	0.00	0.00	0.00	0.44	0.33
X4	−0.10	39.61	0.00	0.00	−0.11	0.69	−0.71
	−0.41	33.02	0.00	−0.25	0.00	−0.31	0.00
X5	−0.69	0.64	0.00	0.00	−0.14	0.14	−1.25
X6	−0.08	0.68	0.00	−0.19	0.00	0.10	−0.40

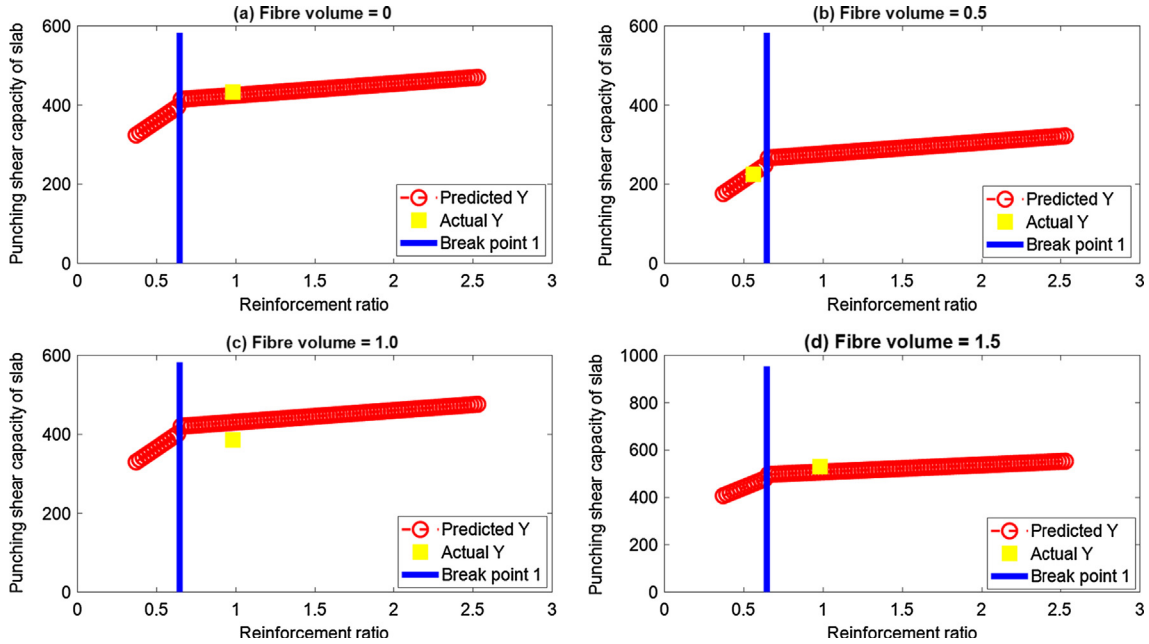

Fig. 10. Visualization of the relationship among the reinforcement ratio, fibre volume, and punching shear strength.

Case 3 (Fig. 10c): $X_1 = 152$, $X_2 = 127$, $X_3 = 152$, $X_4 = 25.4$, $X_5 = 0.98$, $X_6 = 1$, and $Y = 386$.

Case 4 (Fig. 10d): $X_1 = 152$, $X_2 = 127$, $X_3 = 152$, $X_4 = 59.3$, $X_5 = 0.98$, $X_6 = 1.5$, and $Y = 530$.

In Fig. 10, the value of the reinforcement ratio (X_5) are allowed to vary from its minimum and maximum values; other explanatory variables are kept fixed to compute the value of the punching shear strength corresponding to the variation of the reinforcement ratio. As shown in Fig. 10, the relationships of the reinforcement ratio and the punching shear strength can be described by linear models in each domain specified by the breaking points. Moreover, the actual measured punching shear strength values in all the four case are relatively close to the predicted values. These facts confirm the prediction accuracy of the proposed SPMLR used in punching shear strength estimation.

5. Conclusion

This study has constructed machine learning based alternatives for estimating the punching shear capacity of SFRC flat slabs. The proposed approach relies on the SPMLR and ANN models for approximating the mapping function between a set of six explanatory variables (slab depth, effective depth of the slab, length or radius of the loading pad or column, compressive strength of concrete, the reinforcement ratio, and the fibre volume) and the response variable of the punching shear capacity. Gradient descent and Levenberg-Marquardt backpropagation algorithms are used to train the ANN models. Meanwhile, the SPMLR model implements a sequential method to select appropriate breaking points for each explanatory variable.

In addition, three criteria of breaking point selection have been attempted for establishing the SPMLR model structure. Experimental results show that the third criterion that involves the computation of R-RMSE for both training and validating data helps to gain the most desired prediction model. Based on a repeated random subsampling data with 20 runs, it is able to confirm that the SPMLR performance is superior to other benchmark approaches including ANN, MLR, and prediction equations. Besides the aspect of prediction accuracy, the structure of SPMLR is also easier to be interpreted and visualized than that of ANN.

Therefore, the proposed SPMLR can be a promising tool to assist structural engineers in the task of designing SFRC flat slabs. Future extensions of the current study may include the investigation of other breaking point acceptance criteria and other advanced method for overfitting prevention. In addition, the new prediction models should be verified by an extended data set which collects experiments performed in recent studies. Finally, applying the cur-

rent SPMLR model to solve other problems in civil engineering can also be worth-attempting.

Appendix 1. Prediction formulas for computing punching shear strength of SFRC slabs

The punching shear strength of SFRC flat slabs can be estimated by the mechanical model of the critical shear crack theory (CSCT) according to the descriptions of Aurelio [54] for the case of slabs without transverse reinforcement and Fernández Ruiz and Muttoni [55] for the case of slabs with transverse reinforcement. As put forward by [55], the punching shear strength of reinforced concrete slabs without transverse reinforcement presented as follows:

$$V_{R,c} = \frac{3}{4} b_o d \sqrt{f_c} \frac{1}{\left(1 + 15 \frac{\psi d}{d_{g0} + d_g}\right)} \quad (A1)$$

where ψ denotes the maximal rotation of the slab; d is the effective depth of the slab; b_o represents the control perimeter at a distance of $d/2$ from the face of the column; f_c denotes the concrete compressive strength, d_g and d_{g0} are the aggregate size and a reference aggregate size set to 16 mm, respectively.

Because along the failure surface defined by the critical shear crack, total shear strength gains the contribution from both the concrete and the steel fibres [56], the punching shear strength can be computed as follows:

$$V_R = V_{R,C} + V_{R,f} \quad (A2)$$

where $V_{R,c}$ and $V_{R,f}$ are the contributions of the concrete and fibres, respectively.

Voo and Foster [57] proposed an equation to quantify the tensile strength provided by the fibres over a plane of unit area as follows:

$$\sigma_{tf} = K_f . \alpha_f . \rho_f . \tau_b \quad (A3)$$

where K_f denotes the global orientation factor; ρ_f represents the fibre volume, τ_b denotes the bond stress between the fibres and the concrete matrix; α_f is the parameter which specifies the aspect ratio of the steel fibres.

Based on the aforementioned equation, the total punching shear contribution of the fibres can be calculated in the following way [3]:

$$V_{R,f} = \int_{A_p} \sigma_{tf}(\psi, \zeta) dA_p \quad (A4)$$

where ζ denotes the distance of a point with respect to the soffit of the slab; A_p represents the horizontally projected area of the punching shear failure surface. It is noted that the integration described in Eq. (A4) can help to obtain a close-form solution for computing the fibre contribution [56].

Additionally, based on the concept of average bridging stress and the kinematic assumption [56], the fibre contribution can also be computed according to the following equation [3]:

$$V_{R,f} = A_p \sigma_{tf} \left(\frac{\psi d}{6}\right) \quad (A5)$$

Based on Eq. (A5), Maya, Fernández Ruiz, Muttoni and Foster [3] put forward simplified formulation to compute the concrete contribution as follows:

$$V_{R,c} = \frac{2 b_o d \sqrt{f_c}}{3 \gamma_c} \frac{1}{1 + 20 \frac{\psi d}{d_{g0} + d_g}} \quad (A6)$$

where γ_c is the partial safety factor of concrete and equal to 1.5.

Appendix 2. The data set of punching shear capacity

Specimen	X_1	X_2	X_3	X_4	X_5	X_6	Y
Cheng and Parra-Montesinos [12]							
S1	152	127	152	47.7	0.98	0	433
S2	152	127	152	47.7	0.66	0	379
S3/FRC	152	127	152	25.4	0.98	1	386
S4/FRC	152	127	152	25.4	0.66	1	389
S5/FRM	152	127	152	59.3	0.98	1.5	530
S6/FRM	152	127	152	57.9	0.66	1.5	444
S7/FRC	152	127	152	31	0.98	1.5	522
S8/FRC	152	127	152	31	0.66	1.5	472
S9/FRC	152	127	152	46.1	0.98	1.5	530
S10/FRC	152	127	152	59.1	0.66	1.5	503
Theodorakopoulos and Narayan [58]							
FS-1	125	100	150	35.4	0.56	0	173.5
FS-2	125	100	150	34	0.56	0.5	225
FS-3	125	100	150	35.6	0.56	1	247.4
FS-4	125	100	150	35.7	0.56	1	224.4
FS-5	125	100	150	38	0.37	1	198.1
FS-6	125	100	150	35.7	0.37	1	174.5
FS-7	125	100	150	36.6	0.37	1	192.4
FS-19	125	100	150	34.5	0.37	0	136.5
FS-20	125	100	150	37	0.37	1	211
FS-8	125	100	100	36.7	0.56	0	150.3
FS-9	125	100	100	35.6	0.56	1	216.6
FS-10	125	100	200	36.4	0.56	0	191.4
FS-11	125	100	200	34.2	0.56	1	259.8
FS-12	125	100	150	36.1	0.56	1	217.5
FS-13	125	100	150	33.5	0.56	1	235.5
FS-14	125	100	150	35	0.56	1	239.5
FS-15	125	100	150	31.2	0.56	1	238
FS-16	125	100	150	27.9	0.56	1	227.8
FS-17	125	100	150	46.8	0.56	1	268.4
FS-18	125	100	150	14.2	0.56	1	166
Alexander and Simmonds [59]							
P11F0	155	132.7	200	33.2	0.5	0	257
P11F31	155	132.7	200	35.8	0.5	0.39	324
P11F66	155	132.7	200	35	0.5	0.84	345
P38F0	155	105.7	200	38.1	0.63	0	264
P38F34	155	105.7	200	38.4	0.63	0.43	308
P38F69	155	105.7	200	38.5	0.63	0.88	330
De-Hanai and Holanda [60]							
L1	100	80	80	23.1	1.56	0	137.2
L2	100	80	80	24.4	1.56	1	139.6
L3	100	80	80	28.1	1.56	2	163.6
L4	100	80	80	57	1.56	0	192.9
L5	100	80	80	59.7	1.56	1	215.1
L6	100	80	80	52.4	1.56	2	236.2
OSC-S1	100	80	80	43.7	1.56	0	176.5
L7	100	80	80	36.6	1.56	0.75	182.5
L8	100	80	80	46.1	1.56	1.5	210.9
Swamy and Ali [61]							
S-1	125	100	150	37.8	0.56	0	197.7
S-2	125	100	150	39	0.56	0.6	243.6
S-3	125	100	150	37.8	0.56	0.9	262.9
S-4	125	100	150	36.9	0.56	1.2	281
S-5	125	100	150	37.8	0.56	0.9	267.2
S-6	125	100	150	38	0.56	0.9	239
S-7	125	100	150	38.9	0.74	0	221.7
S-13	125	100	150	39.3	0.74	0.9	236.7
S-12	125	100	150	36.8	0.74	0.9	249
S-11	125	100	150	37.1	0.74	0.9	262

Appendix 2 (*continued*)

Specimen	X_1	X_2	X_3	X_4	X_5	X_6	Y
S-8	125	100	150	41.1	0.74	0.9	255.7
S-16	125	100	150	38.9	0.56	0.9	213
S-10	125	100	150	38.9	0.46	0.9	203
S-9	125	100	150	38.9	0.37	0.9	179.3
S-19	125	100	150	38.9	0.37	0	130.7
McHarg, Cook, Mitchell and Yoon [62]							
NU	150	109	225	30	1.12	0	306
NB	150	109	225	30	2.18	0	349
FSU	150	109	225	41.5	1.12	0.5	422
FSB	150	109	225	41.5	2.18	0.5	438
Suter and Moreillon [63]							
B1-01	120	90	60	99	0.87	0	262
B2-01	120	90	60	103	0.87	0.25	318
B3-01	120	90	60	108	0.87	0.51	343
B4-01	120	90	60	106	0.87	0.76	337
B5-01	120	90	60	107	0.87	1.02	369
B1-05	120	92	60	99	0.55	0	201
B3-05	120	92	60	108	0.55	0.51	286
B5-05	120	92	60	107	0.55	1.02	327
B1-06	120	88	60	99	1.29	0	252
B3-06	120	88	60	108	1.29	0.51	361
B5-06	120	88	60	107	1.29	1.02	402
Nguyen-Minh, Rovňák and Tran-Quoc [64]							
A0	125	105	200	21.7	0.66	0	284
A1	125	105	200	22.3	0.66	0.4	330
A2	125	105	200	23.4	0.66	0.6	345
A3	125	105	200	25.3	0.66	0.8	397
B0	125	105	200	21.7	0.66	0	301
B1	125	105	200	22.3	0.66	0.4	328
B2	125	105	200	23.4	0.66	0.6	337
B3	125	105	200	25.3	0.66	0.8	347
C0	125	105	200	21.7	0.66	0	264
C1	125	105	200	22.3	0.66	0.4	307
C2	125	105	200	23.4	0.66	0.6	310
C3	125	105	200	25.3	0.66	0.8	326
Harajli, Maalouf and Khatib [15]							
A1	55	39	100	29.6	1.12	0	58.8
A2	55	39	100	30	1.12	0.45	63.6
A3	55	39	100	31.4	1.12	0.8	73.1
A4	55	39	100	24.6	1.12	1	64.7
A5	55	39	100	20	1.12	2	58.3
B1	75	55	100	31.4	1.12	0	91.8
B2	75	55	100	31.4	1.12	0.45	105.9
B3	75	55	100	31.8	1.12	0.8	108.4
B4	75	55	100	29.1	1.12	1	108.8
B5	75	55	100	29.2	1.12	2	134.5
Yaseen [65]							
S11	60	44	100	35.4	1.61	0.5	89.5
S12	60	44	100	49.1	1.61	0.5	102.5
S13	60	44	100	55.1	1.61	0.5	129.5
S14	60	44	100	65.1	1.61	0.5	141
S21	60	44	100	42.2	1.61	0	93.3
S22	60	44	100	48.8	1.61	0.25	98
S23	60	44	100	52.4	1.61	0.75	125.5
S24	60	44	100	53.3	1.61	1	138
S31	60	44	100	49.2	1.61	0.5	98
S32	60	44	100	49.2	1.61	0.5	100
S33	60	44	100	52.8	1.61	0.5	117.5
S34	60	44	100	49.5	1.61	0.5	110
S41	60	44	75	51.1	1.61	0.5	88.5
S42	60	44	150	50.8	1.61	0.5	135

Appendix 2 (*continued*)

Specimen	X_1	X_2	X_3	X_4	X_5	X_6	Y
Narayanan and Darwish [14]							
S1	60	45	100	43.3	1.84	0	86.5
S2	60	45	100	52.1	1.84	0.25	93.4
S3	60	45	100	44.7	1.84	0.5	102
S4	60	45	100	46	1.84	0.75	107.5
S5	60	45	100	53	1.84	1	113.6
S6	60	45	100	53	1.84	1.25	122.2
S7	60	45	100	47	1.6	1	92.6
S8	60	45	100	45.3	2.08	1	111.1
S9	60	45	100	43.5	2.3	1	111.3
S10	60	45	100	47.6	2.53	1	111.3
S11	60	45	100	29.8	1.84	1	82.1
S12	60	45	100	32.4	1.84	1	84.9
Hiroshi Higashiyama and Mutsumi [66]							
t100-0.67	100	70	100	24.6	0.85	0.67	137.5
t140-0.67	140	110	100	24.6	0.54	0.67	210.2
t180-0.67	180	150	100	24.6	0.4	0.67	297.6
t100-0.72	100	65	100	42.4	0.91	0.72	140.8
t140-0.72	140	105	100	42.4	0.57	0.72	213.2
t180-0.72	180	145	100	42.4	0.41	0.72	290.7
t100-0.91	100	65	100	21.6	0.91	0.91	120.8
t140-0.91	140	105	100	21.6	0.57	0.91	183.1
t180-0.91	180	145	100	21.6	0.41	0.91	231.2
t100-0.63	100	70	100	27.8	0.85	0.63	152.3
t100-0.94	100	70	100	31.1	0.85	0.94	147.9
t100-1.03	100	70	100	30.4	0.85	1.03	158.9
Wang, Tian, Huang, Zhou and Zhao [67]							
S1	120	100	200	17.4	0.98	0	255
S2	120	100	200	19.6	0.98	1	290
S3	120	100	200	20.2	0.98	1.5	315
S4	120	100	200	15	0.98	1	285
S5	120	100	200	14.9	0.98	1.5	310

References

[1] F. Habibi, E. Redl, M. Egberts, W.D. Cook, D. Mitchell, Assessment of CSA A23.3 structural integrity requirements for two-way slabs, Can. J. Civ. Eng. 39 (2012) 351–361.

[2] Y.M. Miguel Fernandez Ruiz, M. Aurelio, Post-punching behavior of flat slabs, Struct. J. 110 (2013) 801–812.

[3] L.F. Maya, M. Fernández Ruiz, A. Muttoni, S.J. Foster, Punching shear strength of steel fibre reinforced concrete slabs, Eng. Struct. 40 (2012) 83–94.

[4] A. Marí, A. Cladera, E. Oller, J.M. Bairán, A punching shear mechanical model for reinforced concrete flat slabs with and without shear reinforcement, Eng. Struct. 166 (2018) 413–426.

[5] J.M. Russell, J.S. Owen, I. Hajirasouliha, Nonlinear behaviour of reinforced concrete flat slabs after a column loss event, Adv. Struct. Eng. 21 (2018) 2169–2183.

[6] A.S. Genikomsou, M.A. Polak, 3D finite element investigation of the compressive membrane action effect in reinforced concrete flat slabs, Eng. Struct. 136 (2017) 233–244.

[7] I. Schousboe, Bailey's crossroads collapse reviewed, J. Constr. Div. 102 (1976) 365–378.

[8] S. King, N.J. Delatte, Collapse of 2000 Commonwealth Avenue: punching shear case study, J. Perform. Constr. Facil 18 (2004) (2000) 54–61.

[9] A.A. Shah, Y. Ribakov, Recent trends in steel fibered high-strength concrete, Mater. Des. 32 (2011) 4122–4151.

[10] K.H. Tan, A. Venkateshwaran, Punching shear in steel fibre reinforced concrete slabs without traditional reinforcement, IOP Conf. Ser.: Mater. Sci. Eng. 246 (2017) 012025.

[11] J.O.J. Ying Tian, B. Oguzhan, Strength evaluation of interior slab-column connections, Struct. J. 105 (2008) 692–700.

[12] M.-Y. Cheng, G.J. Parra-Montesinos, Evaluation of steel fiber reinforcement for punching shear resistance in slab-column connections – part i: monotonically increased load, Struct. J. 107 (2010) 101–109.

[13] ACI, ACI Committee 318. Building code requirements for structural concrete (ACI 318–011) and commentary (ACI 318R–11), Farmington Hills (MI): American Concrete Institute, (2011).

[14] R. Narayanan, I.Y.S. Darwish, Punching shear tests on steel-fibre-reinforced micro-concrete slabs, Mag. Concr. Res. 39 (1987) 42–50.
[15] M.H. Harajli, D. Maalouf, H. Khatib, Effect of fibers on the punching shear strength of slab-column connections, Cem. Concr. Compos. 17 (1995) 161–170.
[16] K.-K. Choi, M.M. Reda Taha, H.-G. Park, A.K. Maji, Punching shear strength of interior concrete slab–column connections reinforced with steel fibers, Cem. Concr. Compos. 29 (2007) 409–420.
[17] N.D. Gouveia, N.A.G. Fernandes, D.M.V. Faria, A.M.P. Ramos, V.J.G. Lúcio, SFRC flat slabs punching behaviour – Experimental research, Compos. B Eng. 63 (2014) 161–171.
[18] N.D. Gouveia, M. Lapi, M. Orlando, D.M.V. Faria, A.M.P. Ramos, Experimental and theoretical evaluation of punching strength of steel fiber reinforced concrete slabs, Struct. Concr. 19 (2018) 217–229.
[19] N.D. Gouveia, D.M.V. Faria, A. PinhoRamos, Assessment of SFRC flat slab punching behaviour – Part I: monotonic vertical loading, Mag. Concr. Res. (2018) 1–12.
[20] N.D. Gouveia, D.M.V. Faria, A.P. Ramos, Assessment of SFRC flat slab punching behaviour – part II: reversed horizontal cyclic loading, Mag. Concr. Res. 71 (2019) 26–42.
[21] D. Kueres, M. Ricker, M. Classen, J. Hegger, Fracture kinematics of reinforced concrete slabs failing in punching, Eng. Struct. 171 (2018) 269–279.
[22] D. Kueres, J. Hegger, Two-parameter kinematic theory for punching shear in reinforced concrete slabs without shear reinforcement, Eng. Struct. 175 (2018) 201–216.
[23] J. Einpaul, M.F. Ruiz, A. Muttoni, Measurements of internal cracking in punching test slabs without shear reinforcement, Mag. Concr. Res. 70 (2018) 798–810.
[24] J.T. Simões, M. Fernández Ruiz, A. Muttoni, Validation of the Critical Shear Crack Theory for punching of slabs without transverse reinforcement by means of a refined mechanical model, Struct. Concr. 19 (2018) 191–216.
[25] M.H. Rafiei, H. Adeli, A novel machine learning-based algorithm to detect damage in high-rise building structures, Struct. Des. Tall Spec. Build. 26 (2017) 1–11.
[26] W.Z. Taffese, E. Sistonen, Machine learning for durability and service-life assessment of reinforced concrete structures: Recent advances and future directions, Autom. Constr. 77 (2017) 1–14.
[27] H. Salehi, R. Burgueño, Emerging artificial intelligence methods in structural engineering, Eng. Struct. 171 (2018) 170–189.
[28] Ł. Sadowski, J. Hoła, S. Czarnecki, D. Wang, Pull-off adhesion prediction of variable thick overlay to the substrate, Autom. Constr. 85 (2018) 10–23.
[29] D.-T. Vu, N.-D. Hoang, Punching shear capacity estimation of FRP-reinforced concrete slabs using a hybrid machine learning approach, Struct. Infrastruct. Eng. 12 (2016) 1153–1161.
[30] A. Goetzke-Pala, A. Hoła, Ł. Sadowski, A non-destructive method of the evaluation of the moisture in saline brick walls using artificial neural networks, Arch. Civ. Mech. Eng. 18 (2018) 1729–1742.
[31] N.-D. Hoang, An artificial intelligence method for asphalt pavement pothole detection using least squares support vector machine and neural network with steerable filter-based feature extraction, Adv. Civ. Eng. 2018 (2018) 1–12.
[32] D. Tien Bui, V.-H. Nhu, N.-D. Hoang, Prediction of soil compression coefficient for urban housing project using novel integration machine learning approach of swarm intelligence and Multi-layer Perceptron Neural Network, Adv. Eng. Inf. 38 (2018) 593–604.
[33] S. Weisberg, Applied Linear Regression, Third Edition., John Wiley & Sons, Printed in the United States of America, 2005.
[34] S.E. Ryan, L.S. Porth, A tutorial on the piecewise regression approach applied to bedload transport data, Gen. Tech. Rep. RMRS-GTR-189. Fort Collins, CO: U.S. Department of Agriculture, For. Serv., Rocky Mt. Res. Station 41 (2007) p.
[35] E. Papadimitriou, V. Mylona, J. Golias, Perceived level of service, driver, and traffic characteristics: piecewise linear model, J. Transp. Eng. 136 (2010) 887–894.
[36] M.E. Greene, O. Rolfson, G. Garellick, M. Gordon, S. Nemes, Improved statistical analysis of pre- and post-treatment patient-reported outcome measures (PROMs): the applicability of piecewise linear regression splines, Qual. Life Res. 24 (2015) 567–573.
[37] B.A. Trenholm, A least squares algorithm for fitting piecewise linear functions on fixed domains, Defence Research Reports, DREA-TM-85-215 — Technical, Memorandum (1985).
[38] S. Shi, Y. Li, C. Wan, Robust continuous piecewise linear regression model with multiple change points, J. Supercomputing (2018) 1–23.
[39] J. Pittman, C.A. Murthy, Fitting optimal piecewise linear functions using genetic algorithms, IEEE Trans. Pattern Anal. Mach. Intell. 22 (2000) 701–718.
[40] M.A. García, F. Rodríguez, An iterative algorithm for automatic fitting of continuous piecewise linear models, J. WSEAS Trans. Signal Process. 4 (2008) 474–483.
[41] L. Yang, S. Liu, S. Tsoka, L.G. Papageorgiou, Mathematical programming for piecewise linear regression analysis, Expert Syst. Appl. 44 (2016) 156–167.
[42] A. Toriello, J.P. Vielma, Fitting piecewise linear continuous functions, Eur. J. Oper. Res. 219 (2012) 86–95.
[43] A.A. Chojaczyk, A.P. Teixeira, L.C. Neves, J.B. Cardoso, C. Guedes Soares, Review and application of Artificial Neural Networks models in reliability analysis of steel structures, Struct. Saf. 52 (2015) 78–89.
[44] B. Gordan, M. Koopialipoor, A. Clementking, H. Tootoonchi, E. Tonnizam Mohamad, Estimating and optimizing safety factors of retaining wall through neural network and bee colony techniques, Eng. Comput. (2018) 1–10.
[45] S. Chatterjee, S. Sarkar, S. Hore, N. Dey, A.S. Ashour, V.E. Balas, Particle swarm optimization trained neural network for structural failure prediction of multistoried RC buildings, Neural Comput. Appl. 28 (2017) 2005–2016.
[46] U.K. Mallela, A. Upadhyay, Buckling load prediction of laminated composite stiffened panels subjected to in-plane shear using artificial neural networks, Thin-Walled Struct. 102 (2016) 158–164.
[47] V.K. Ojha, A. Abraham, V. Snášel, Metaheuristic design of feedforward neural networks: A review of two decades of research, Eng. Appl. Artif. Intell. 60 (2017) 97–116.
[48] C.M. Bishop, Pattern Recognition and Machine Learning (Information Science and Statistics) Springer (April 6, 2011), ISBN-10: 0387310738, 2011.
[49] D.E. Rumelhart, G.E. Hinton, R.J. Williams, Learning representations by back-propagating errors, Nature 323 (1986) 533–536.
[50] J. Heaton, Artificial Intelligence for Humans, Volume 3 Deep Learning and Neural Networks, Heaton Research, Inc., United States, 2015.
[51] M.T. Hagan, M.B. Menhaj, Training feedforward networks with the Marquardt algorithm, IEEE Trans. Neural Networks 5 (1994) 989–993.
[52] Matwork, Statistics and Machine Learning Toolbox User's Guide, Matwork Inc., https://www.mathworks.com/help/pdf_doc/stats/stats.pdf, Date of last access: 04/28/2018, 2017.
[53] L. Breiman, Hinging hyperplanes for regression, classification, and function approximation, IEEE Trans. Inf. Theory 39 (1993) 999–1013.
[54] M. Aurelio, Punching Shear Strength of Reinforced Concrete Slabs without Transverse Reinforcement, Struct. J. 105 (2008) 440–450.
[55] M.F. Ruiz, A. Muttoni, Applications of Critical Shear Crack Theory to Punching of Reinforced Concrete Slabs with Transverse Reinforcement, Struct. J. 106 (2009) 485–494.
[56] A. Muttoni, M.F. Ruiz MC2010 – the critical shear crack theory as a mechanical model for punching shear design and its application to code provisions, in: FIB Bulletin 57: shear and punching shear in RC and FRC elements. Lausanne (Switzerland), (2010) 31–60.
[57] J.Y.L. Voo, S.J. Foster, Tensile fracture of fibre reinforced concrete: variable engagement model, in: 6th Rilem symposium of fibre reinforced, concrete (FRC). Varenna (Italy); 2004. p. 875–84, (2004).
[58] D.D. Theodorakopoulos, S. Narayan, Contribution of steel fibers to the strength characteristics of lightweight concrete slab-column connections failing in punching shear, Struct. J. 90 (1993) 342–355.
[59] S.D.B. Alexander, S.H. Simmonds, Punching shear tests of concrete slab-column joints containing fiber reinforcement, Struct. J. 89 (1992) 425–432.
[60] J.B. De-Hanai, K.M.A. Holanda, Similarities between punching and shear strength of steel fiber reinforced concrete (SFRC) slabs and beams, IBRACON 1 (2008) 1–16.
[61] R.N. Swamy, S.A.R. Ali, Punching shear behavior of reinforced slab-column connections made with steel fiber concrete, J. Proc. 79 (1982) 392–406.
[62] P.J. McHarg, W.D. Cook, D. Mitchell, Y.S. Yoon, Benefits of concentrated slab reinforcement and steel fibers on performance of slab-column connections, ACI Struct. J. 97 (2000) 225–234.
[63] R. Suter, L. Moreillon, Punching shear strength of high performance fiber reinforced concrete slabs, in: Proc. of the 3rd FIB international congress, Washington (USA), (2010).
[64] L. Nguyen-Minh, M. Rovňák, T. Tran-Quoc, Punching Shear Capacity of Interior SFRC Slab-Column Connections, J. Struct. Eng. 138 (2012) 613–624.
[65] A. Yaseen, Punching shear strength of steel fiber high strength reinforced concrete slabs, Master Thesis, College of Engineering University of Salahaddin, Erbil (Iraq), 2006.
[66] A.O. Hiroshi Higashiyama, M. Mutsumi, Design equation for punching shear capacity of sfrc slabs, IJCSM 5 (2011) 35–42.
[67] X.W. Wang, W.L. Tian, Z.Y. Huang, M.J. Zhou, X.Y. Zhao, Analysis on punching shear behavior of the raft slab reinforced with steel fibers, Key Eng. Mater. 400–402 (2009) 335–340.